Spatiotemporal evolution of ultrafast magnetic-field generation in molecules with intense bichromatic circularly polarized UV laser pulses

Jing Guo,[1] Kai-Jun Yuan,[1,2,*] Huizhong Lu,[2] and André D Bandrauk[2,†]

[1]*Institute of Atomic and Molecular Physics, Jilin University, Changchun 130012, China*

[2]*Laboratoire de Chimie Théorique, Faculté des Sciences, Université de Sherbrooke, Sherbrooke, Québec, Canada J1K 2R1*

(Received 20 December 2018; published 20 May 2019)

We present ultrafast magnetic-field pulse generation in aligned molecules from numerical solutions of time-dependent Schrödinger equations. The one-electron molecular ion H_2^+ as a benchmark model is used to describe the ultrafast photophysics process. Schemes with bichromatic high-frequency corotating and counterrotating $(\omega, 2\omega)$ and $(\omega, 3\omega)$ circularly polarized UV laser pulses are presented to produce the spatial and temporal evolution of the generated magnetic field. We discuss how interference effects between multiple resonant excitations modulate the evolution of the generated magnetic field. It is found that the modulation of generated magnetic fields is dependent on the pulse frequency and helicity combination and the molecular alignment, which is attributed to the different resonant excitation processes with various molecular orbitals that vary the intramolecular coherent electron currents. The spatiotemporal evolution of generated magnetic fields is shown to be related and strongly different for molecular around-axis and in-plane electron currents. The scheme allows one to control the induced magnetic-field-pulse generation as a tool for ultrafast optical magnetism.

DOI: 10.1103/PhysRevA.99.053416

I. INTRODUCTION

Controlling electron dynamics with intense ultrashort laser pulses on its natural timescale, the attosecond (1 asec = 10^{-18} s) since the $1s$ H atom orbit period is 152 asec, has motivated the birth of a new science, attosecond physics [1,2]. To date 43 asec pulses are the shortest available pulse for new ultrafast optical imaging [3]. With mid-infrared femtosecond lasers, high-order harmonic generation (HHG) spectra of very high order 5000 (1.6 keV) can also be generated thus allowing for the generation of pulses as short as a few attoseconds [4]. With these new attosecond pulses electrons can therefore be visualized and controlled on the attosecond timescale and subnanometer dimension in atoms, molecules, and surfaces [5–10]. However the development of attosecond pulse technology has been limited to linear polarization. Circularly polarized attosecond pulses have been now proposed as future tools for studying attosecond electron currents and their dynamics in atoms [11–14] and molecules [15–17]. A drawback of single circularly polarized pulses is the suppression of recollision of ionized electrons with parent ions contrary to linearly polarized pulses, where laser-induced recollision generates HHG [18]. Combinations of bichromatic circularly polarized pulses were predicted as early as 1995 to generate harmonics due to enhanced ionized electron-parent ion recombination [19,20] allowing one to generate circularly polarized harmonics, e.g., [21–24], from which one can generate circularly polarized attosecond pulses [25].

The science of magneto-optics is currently influenced by the discovery that magnetic polarization of atoms in matter is controllable, generated and monitored by ultrafast laser pulses on the femtosecond (1 fs = 10^{-15} s) timescale, the timescale of atomic motion in matter [26–28]. Recently, the generation of electronic ring currents in aromatic molecules obtained from quantum-chemical numerical simulations have produced static magnetic fields by means of linearly and circularly polarized UV pulses resonant with degenerate π molecular orbitals [29–32]. The generated magnetic fields can be much larger than those obtained by traditional static fields. It has been found that the generated magnetic field from electronic rings in atomic orbitals is strongly dependent on the quantum numbers and the nuclear charge [32]. The strategy allows one to produce strong magnetic fields by controlling the orbital angular momentum in atoms and molecules. In these previous studies, coherent rotational electronic states are prepared resonantly, thus leading to static magnetic fields. Moreover the induced currents have been found to rely strongly on the coherence of the excited states [33], allowing one to reconstruct molecular attosecond charge migration [34,35] via the control of electron-state symmetry [36,37].

Coherent circular electronic wave packets in quasicontinua induce temporal coherent electron currents, giving rise to time-dependent magnetic fields [38–41]. In the present work, we study the spatiotemporal evolution of the magnetic-field-pulse generation by intense bichromatic circularly polarized UV laser pulses. Simulations are performed on the benchmark molecule H_2^+ [42] by numerically solving the corresponding time-dependent Schrödinger equation (TDSE). The evolution of the generated magnetic field in spatiotemporal space is shown to be dependent on the molecular alignment and the pulse frequency and helicity combination, reflecting the ultrafast coherent electron excitation dynamics in molecules. Various molecular excited state orbitals give rise to different

*kaijun.yuan@usherbrooke.ca

†andre.bandrauk@usherbrooke.ca

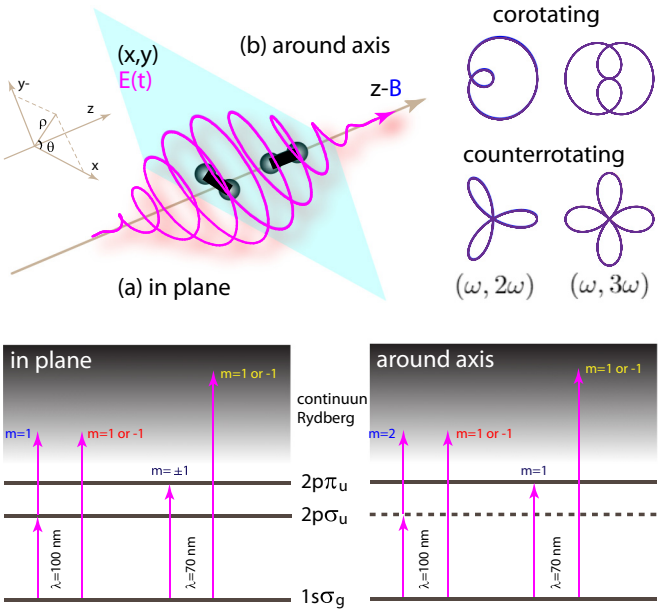

FIG. 1. Upper row: Illustration of time-dependent magnetic field generation in the molecular ion H_2^+ by bichromatic circularly polarized laser pulses with their field polarization vectors in the $(x = \rho\cos\theta, y = \rho\sin\theta)$ plane, propagating along the z axis, for the two cases (a) in-plane, the molecule aligned along the x axis, $R \parallel (x, y)$, and (b) around-axis, the molecule aligned along the z axis, $R \perp (x, y)$. The pulses with co- and counterrotating components and frequency combinations $(\omega, 2\omega)$ and $(\omega, 3\omega)$ are used to induce electron currents in molecules, leading to magnetic fields along the z axis. Bottom row: The possible photoexcitation and photoionization pathways to produce coherent electron currents and magnetic fields by bichromatic $(\omega, 2\omega)$ circularly polarized laser pulses. The excited-state orbitals (m) depend on the molecular alignment and the pulse frequency and helicity combinations.

coherent electron currents. We focus on the frequency combinations $(\omega, 2\omega)$ and $(\omega, 3\omega)$ of bichromatic circular pulses for which the net electric fields have distinct symmetries, as illustrated in Fig. 1, which can be used to generate currents with symmetry [43]. Such a combination of ultrafast circularly polarized pulses can lead to recollision of electrons with parent ions [44], which has been recently used to develop bicircular high-harmonic spectrometry in atoms and molecules for exploring dynamical symmetries [45] and generating polarized attosecond pulses [46]. Time-delayed opposite-helicity circularly polarized pulses have been also investigated in atoms to produce, by single-photon and multiphoton ionization electron vortices in atomic [47,48] and molecular [49] systems, new electronic photoionization patterns. Here we find that using bichromatic circularly polarized UV laser pulses, the interference effects between multiple pathway excitation processes lead to an ultrafast modulation of generated magnetic fields, which is shown to be sensitive to the molecular alignments, as illustrated in Fig. 1. The molecular rotational and vibrational motions on picosecond (1 ps $= 10^{-12}$ s) and femtosecond timescales are ignored because these effects are much slower than the laser-molecule interaction that occurs within the attosecond timescale.

The paper is organized as follows: In Sec. II, we briefly describe the numerical and computational methods. Simulation results obtained by time-dependent quantum electron wave packet calculations for the aligned molecule H_2^+ are presented and discussed in Sec. III. Spatial and temporal evolutions of generated magnetic fields by bichromatic circularly polarized laser pulses correspond to coherent electron excitations. Finally, we summarize our findings in Sec. IV. Throughout this paper, atomic units (a.u.) are used unless otherwise noted.

II. THEORETICAL AND COMPUTATIONAL METHODS

In the present work numerical solutions of TDSEs are used to study the generation of magnetic fields in the molecular ion H_2^+ as a benchmark model that can be investigated completely in both theory and experiment [42] and compared to the molecular alignments parallel and perpendicular to the plane of the laser polarization, as illustrated in Fig. 1. For an aligned single-electron molecular ion H_2^+ within the fixed nuclei (Born-Oppenheimer approximation) frame, Fig. 1, the corresponding TDSE is written as

$$i\frac{\partial}{\partial t}\psi(\mathbf{r}, t) = H(\mathbf{r}, t)\psi(\mathbf{r}, t), \tag{1}$$

where the field-molecule Hamiltonian is $H(\mathbf{r}, t) = T(\mathbf{r}) + V(\mathbf{r}) + \mathbf{r}\cdot\mathbf{E}(t)$ and $\mathbf{r} = (\rho, \theta, z)$ with $(x = \rho\cos\theta,\ y = \rho\sin\theta)$. $V(\mathbf{r})$ is the two-center molecular Coulomb potential. We use cylindrical coordinates $\mathbf{r} = (\rho, \theta, z)$ to describe the electron dynamics in the laser polarization (x, y) plane, with the molecular center $\mathbf{r} = 0$.

The field-molecule interaction is treated in the length gauge and dipole approximation, since by exact solutions of the TDSE, numerical results are gauge invariant [50]. The laser field $\mathbf{E}(t) = \hat{e}_x E_x(t) + \hat{e}_y E_y(t)$ with polarization vectors $\hat{e}_x$ and $\hat{e}_y$ in the (x, y) plane propagates along the z axis, having the form

$$E(t) = E_0 f(t)\begin{cases}\hat{e}_x[\cos(\omega_1 t) + \cos(\omega_2 t)],\\ \hat{e}_y[\sin(\omega_1 t) + \epsilon\sin(\omega_2 t)],\end{cases} \tag{2}$$

with pulse frequencies ω_1 and ω_2, and helicity components $\epsilon = +1$ for corotating and $\epsilon = -1$ for counterrotating components. $\hat{e}_x$ and $\hat{e}_y$ are the two orthogonal laser polarization directions. A smooth $f(t) = \sin^2(\pi t/n\tau_{1/2})$ pulse envelope for the maximum electric field amplitude E_0, corresponding to intensity $I_0 = cE_0^2/8\pi$, is adopted, where one optical cycle (oc) period $\tau_{1/2} = 2\pi/\omega_{1/2}$.

We solve numerically the 3D TDSE in Eq. (1) of the H_2^+ single-electron molecule system by a five-point finite-difference method and fast Fourier transform (FFT) technique combined with high-order split-operator propagation methods [51,52]. The time step is fixed at $\Delta t = 0.01$ a.u. (1 a.u. $= 24$ asec) and the spatial discretization is $\Delta\rho = \Delta z = 0.25$ a.u. (1 a.u. $= 1a_0$, Bohr radius) for radial grid sizes $0 \leqslant \rho \leqslant 128$ a.u., greater than the maximum electron excursion $\alpha_d = E_0/\omega_{1/2}^2$, $|z| \leqslant 64$ a.u., and angle grid size $\Delta\theta = 0.01$ radians. To prevent unphysical effects due to the reflection of the ionized wave packet from the boundary, a "mask function" with the form $\cos^{1/8}[\pi(\rho - \rho_a)/2\rho_{\rm abs}]$ is used at $\rho_{\rm abs} = \rho_{\rm max} - \rho_a = 24$ a.u. with $\rho_{\rm max} = 128$ a.u.

As illustrated in Fig. 1, the time-dependent magnetic field $B(\mathbf{r},t)$ along the z axis is generated from the induced electronic currents in the laser polarization (x,y) plane by bichromatic circularly polarized attosecond UV laser pulses. The time-dependent electronic current density is defined by the quantum expression also in the length gauge,

$$\mathbf{j}(\mathbf{r},t)=\frac{i}{2}[\psi(\mathbf{r},t)\nabla_{\mathbf{r}}\psi^{*}(\mathbf{r},t)-\psi^{*}(\mathbf{r},t)\nabla_{\mathbf{r}}\psi(\mathbf{r},t)]. \quad (3)$$

$\psi(\mathbf{r},t)$ is the exact Born-Oppenheimer (static nuclei) electron wave function obtained from the TDSE equation (1), and $\nabla_{\mathbf{r}}=\mathbf{e}_{\rho}+\mathbf{e}_{\theta}\frac{1}{\rho}\nabla_{\theta}+\mathbf{e}_{z}\nabla_{z}$ in the cylindrical coordinates. The corresponding time-dependent magnetic field is calculated using the following classical Jefimenko equation [53]

$$\mathbf{B}(\mathbf{r},t)=\frac{\mu_0}{4\pi}\int\left[\frac{\mathbf{j}(\mathbf{r}',t_r)}{|\mathbf{r}-\mathbf{r}'|^3}-\frac{1}{c|\mathbf{r}-\mathbf{r}'|^2}\frac{\partial\mathbf{j}(\mathbf{r}',t_r)}{\partial t}\right]\times(\mathbf{r}-\mathbf{r}')d^3\mathbf{r}', \quad (4)$$

where $t_r=t-r/c$ is the retarded time and $\mu_0=4\pi\times10^7$ N A^{-2} (6.692×10^{-4} a.u.). For static-field time-independent conditions occurring after the pulse, Eq. (4) reduces to the classical Biot-Savart law.

III. RESULTS AND DISCUSSION

The purpose of the present work is to study the magnetic-field generation in molecules by intense bichromatic circular polarization pulses with both corotating and counterrotating components. We use a typical molecule, H_2^+, which is aligned parallel [Fig. 1(a)] or perpendicular [Fig. 1(b)] to the laser propagation direction. In the simulations, the molecule is initially prepared in the ground $1s\sigma_g$ state of the aligned molecule H_2^+ at equilibrium $R_e=2$ a.u. (1.06 Å) with the ionization potential $I_p=1.1$ a.u. (29.72 eV). The initial electron wave function $\psi(\mathbf{r},t=0)$ is obtained by propagating an initial appropriate wave function via the field-free TDSE in imaginary time [52]. We adopt bichromatic circularly polarized pulses in Eq. (2) at frequencies $(\omega_1=\omega,\omega_2=2\omega)$ or $(\omega_1=\omega,\omega_2=3\omega)$ as illustrated in Fig. 1. Each component of the bicircular pulse has intensities $I_x=I_y=3.5\times10^{14}$ W/cm^2 ($E_0=0.1$ a.u.), with wavelength $\lambda=100$ nm ($\omega=0.456$ a.u.), resonant with the $1s\sigma_g$–$2p\sigma_u$ parallel transition, or $\lambda=70$ nm ($\omega=0.65$ a.u.), resonant with the $1s\sigma_g$–$2p\pi_u$ perpendicular transition, and five cycles' duration for each, $5\tau_1=1.667$ fs (100 nm) or $5\tau_2=1.167$ fs (70 nm). The Keldysh parameter $\gamma=\sqrt{I_p/2U_p}$ (in a.u.), for the ponderomotive energy $U_p=I/4\omega^2$ (a.u.), is $\gamma_{x/y}=6.77$ at 100 nm and $\gamma_{x/y}=9.68$ at 70 nm, for each field component, indicating a region of multiphoton ionization processes [1,2].

A. Time-dependent magnetic fields

We first present the evolution of the generated magnetic field with time. To illustrate the effects of coherent electron currents, we compare molecular excitation processes with various pulse frequencies and molecular alignments, which lead to different angular momentum states. Figure 2 illustrates the time-dependent molecular orbital populations of the three lowest $1s\sigma_g$, $2p\sigma_u$, and $2p\pi_u$ electronic states of H_2^+ exposed to monochromatic 70 nm and 100 nm circularly polarized

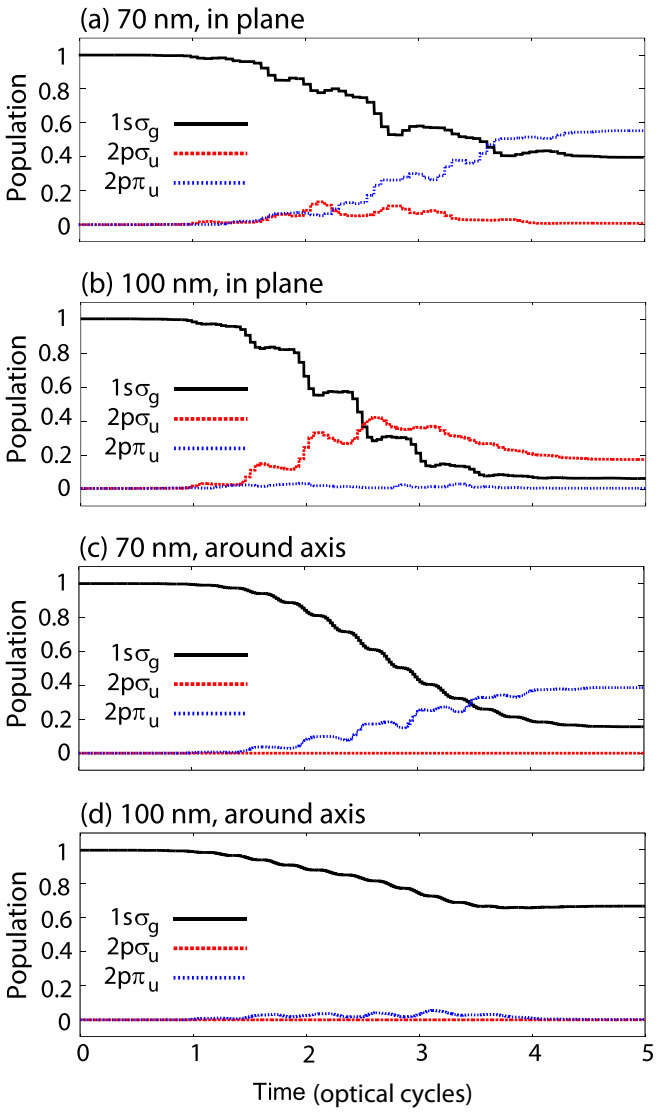

FIG. 2. Time-dependent molecular orbital population in the molecular H_2^+ $1s\sigma_g$, $2p\sigma_u$, and $2p\pi_u$ electronic states by (a), (c) $\lambda=70$ nm and (b), (d) 100 nm monochromatic circularly polarized pulses for the two cases of molecular alignments (a), (b) in plane, the molecular axis $R\parallel x$, the laser polarization plane, and (c), (d) around axis, $R\perp(x,y)$, as illustrated in Fig. 1. The pulse intensity $I_0=3.5\times10^{14}$ W/cm^2 ($E_0=0.1$ a.u.) and duration 5 oc, where 1 optical cycle (oc) $=2\pi/\omega$; i.e., 1.167 fs for $\lambda=70$ nm ($\omega=0.65$ a.u.) and 1.667 fs for $\lambda=100$ nm ($\omega=0.456$ a.u.) are used.

pulses. In Figs. 2(a) and 2(b) the molecular R axis is aligned in the (x,y) polarization plane of the pulse, as in Fig. 1(a), and in Figs. 2(c) and 2(d) the molecular R axis is parallel to the z pulse propagation direction, with the (x,y) field polarization perpendicular to R, Fig. 1(b). Thus for the in-plane excitation ionization Fig. 1(a), at 70 nm one has mainly a $1s\sigma_g$–$2p\pi_u$ perpendicular resonant transition to both degenerate $m=\pm1$ angular momentum states, Fig. 2(a), whereas at 100 nm, the E_x component of the pulse excites mainly the $2p\sigma_u$ state due to change resonance excitation with a transition moment $R/2$ parallel to R [54], leading to enhanced ionization [55]. In fact at 800 nm, charge-resonant enhanced ionization occurs

with in-plane circular polarization as in linear polarization, thus confirming the strong radiative coupling when $E_x \parallel R$ [44,56]. For the 70 nm excitation ionization around the R molecular axis, Fig. 2(c) shows mainly a $1s\sigma_g$–$2p\pi_u^+$ transition to the $m = +1$ angular momentum state around the z/R axis for positive helicity, with negligible $2p\sigma_u$ excitation. For the $\lambda = 100$ nm perpendicular excitation around the R axis, no resonant excitation is expected due to selection rules, and the $1s\sigma_g$ state ionizes directly via Rydberg or continuum states. Comparing the in-plane to the around-axis cases at $\lambda = 70$ nm, Fig. 2(a) vs Fig. 2(c), one notes that the in-plane ionization exceeds the round axis result by nearly a factor of two due to ionization of both $m = +1$ and -1 $2p\pi_u$ states by perpendicular transitions.

In Figs. 3 and 4 we simulate the temporal evolution of the generated magnetic fields $B_z(\mathbf{r} = 0, t)$ at the molecular center of the H_2^+ molecule (Fig. 1) generated by 5-cycle pulses for various wavelengths λ single frequencies ω, and their combinations $(\omega, 2\omega)$, $(\omega, 3\omega)$ with co- and counterrotating components. It is found that the generated magnetic field oscillates with time t on the attosecond timescale. We use the driving circularly polarized laser pulses with their field vectors in the (x, y) plane. The induced electron currents evolve in the (x, y) plane as well. As a result, the generated magnetic fields are mainly along the z axis, perpendicular to the laser polarization plane, as illustrated in Fig. 1. Two cases around the molecular R/z axis, Figs. 3(a) and 4(a), and in the molecular (x, y) plane, Figs. 3(b) and 4(b), are compared. The fundamental pulse wavelengths are used at (Fig. 3) $\lambda = 70$ nm ($\omega = 0.65$ a.u.) and (Fig. 4) $\lambda = 100$ nm ($\omega = 0.456$ a.u.). The strongest magnetic field $B_z(\mathbf{r} = 0, t) = 0.7$ T is obtained in Fig. 3(a), at 70 nm around the z axis as the ω frequency excites resonantly the $2p\pi_u^+$ state and an $m = +1$ electron current in the (x, y) plane around the R molecular axis. The current (population) has a maximum at each optical cycle in agreement with the $2p\pi_u$ population in Fig. 2(b). The counterrotating bichromatic $(\omega, 2\omega)$ and $(\omega, 3\omega)$ circularly polarized pulses (green lines) essentially follow the single ω pulse magnetic fields whereas the corotating pulses (red lines) generate magnetic fields slightly larger than single ω pulses. The in-plane (x, y) currents generate corresponding magnetic fields, Fig. 3(b), which change sign at the middle duration time (~2.5 oc) of all pulses. Minima-maxima occur again at the optical cycles. The main difference at 70 nm between around-axis and in-plane magnetic fields is that around axis, Fig. 3(a), a single magnetic quantum number state $m = +1$ or -1 is excited resonantly whereas for in-plane excitation, Fig. 3(b), both degenerate $m = \pm 1$ states are excited coherently. Of note is that at 3.5 cycles, the 70 nm in-plane magnetic fields have the same intensity as the around-axis magnetic field, Fig. 3(a), but with opposite phases. Figure 4 illustrates magnetic fields generated at 100 nm excitation. It is interesting that, in Fig. 4(a), mainly positive magnetic-field oscillations are generated around the molecular R/z axis, whereas in the molecular (x, y) plane, Fig. 4(b), co- and counterrotating magnetic fields are out of phase. At 100 nm excitation, which is nonresonant with the $1s\sigma_g$–$2p\pi_u$ transition, the E_x and E_y electric-field components are perpendicular to R in circular polarization around the z axis, Fig. 1(b), but in in-plane alignments, Fig. 1(a), E_x is parallel to R, inducing large $2p\sigma_u$ excitation due to charge

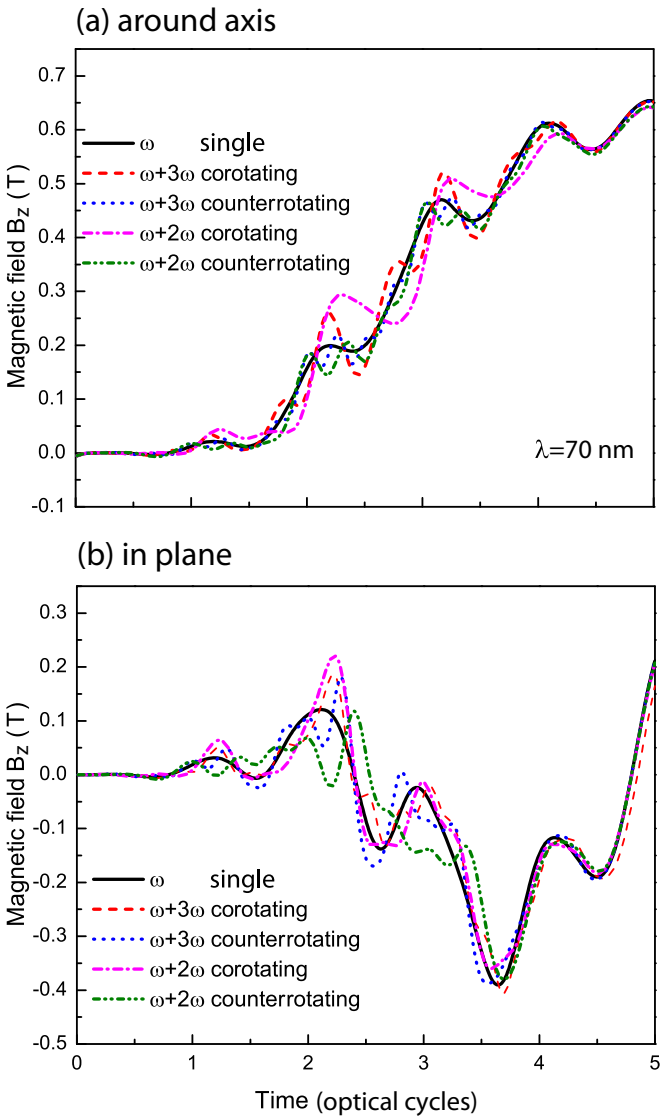

FIG. 3. Temporal evolutions of the generated magnetic field $B_z(\mathbf{r} = 0, t)$ in the molecular ion H_2^+ by bichromatic circularly polarized UV laser pulses with various frequency combinations and co- and counterrotating components. The pulse fundamental frequency $\omega = 0.65$ a.u., corresponding to $\lambda = 70$ nm, leads to a perpendicular $1s\sigma_g$–$2p\pi_u$ resonant excitation. Two cases, (a) around axis and (b) in plane, are compared. The pulse intensity $I_0 = 3.5 \times 10^{14}$ W/cm^2 ($E_0 = 0.1$ a.u.) and duration 5 oc = 1.167 fs, where 1 optical cycle (oc) $= 2\pi/\omega = 232$ asec for $\lambda = 70$ nm, are used.

resonance with no $2p\pi_u$-state excitation, Fig. 2(b). The current symmetries generated by the symmetries of the net $(\omega, 2\omega)$ and $(\omega, 3\omega)$ fields induce strong phase variation in the magnetic fields as illustrated in Fig. 4(b).

Figures 3 and 4 summarize the time-dependent magnetic field $B_z(\mathbf{r} = 0, t)$ generated at the molecular center. The resonant $1s\sigma_g$–$2p\pi_u$ excitation by the 70 nm pulse, Figs. 2(a) and 2(c) with $m = \pm 1$, is dominant in the evolution processes of the magnetic-field generation. As shown in Fig. 3, the magnetic fields oscillate with time t with the same period and amplitude for the frequency combinations $(\omega, 2\omega)$ and $(\omega, 3\omega)$ with both co- and counterrotating components. In

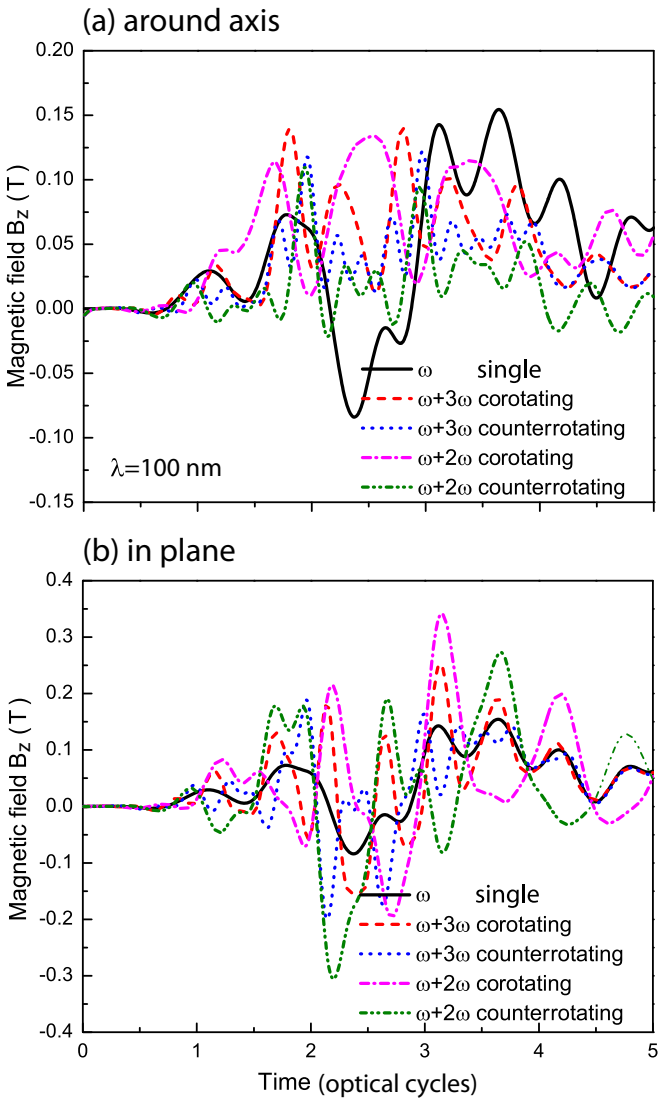

FIG. 4. Temporal evolutions of the generated magnetic field $B_z(\mathbf{r}=0,t)$ in the molecular ion $H_2{}^+$ by bichromatic circularly polarized UV laser pulses with various frequency combinations and co- and counterrotating components. The pulse fundamental frequency $\omega = 0.456$ a.u., corresponding to $\lambda = 100$ nm, leads to a parallel $1s\sigma_g$–$2p\sigma_u$ resonant excitation. Two cases, (a) around axis and (b) in plane, are compared. The pulse intensity $I_0 = 3.5 \times 10^{14}$ W/cm^2 ($E_0 = 0.1$ a.u.) and duration 5 oc = 1.667 fs, where 1 optical cycle (oc) $= 2\pi/\omega = 331$ asec for $\lambda = 100$ nm, are used.

both around-axis [Fig. 3(a)] and in-plane [Fig. 3(b)] processes, higher frequency excitations are negligible. However, as shown in Fig. 4, the generated magnetic field $B_z(\mathbf{r}=0,t)$ is shown to be dependent on the pulse-frequency combination. The time-dependent magnetic fields $B_z(\mathbf{r}=0,t)$ at $\lambda =$ 100 nm (ω) and frequency multiplication 2ω and 3ω pulses in both around-axis and in-plane cases are strongly influenced by the different field symmetries. The modulation illustrates the effects of the interference between the coherent electron wave packets. Such bichromatic laser pulses produce a photoelectron with the same kinetic energies by the two $\omega+\omega$ and one 2ω photon absorption or three $\omega+\omega+\omega$ and one 3ω photon process. As a result, these electron wave packets interfere with each other. In particular, $(\omega, 2\omega)$ and $(\omega, 3\omega)$ corotating and counterrotating pulses create out-of-phase magnetic fields.

We examine next the $(\omega, 2\omega)$ process as an example to describe the ultrafast magnetic field generation. According to the attosecond photoionization perturbation theoretical model, the total transition probability is the square of the two amplitudes with an interference term of the cross products of the two one- and two-photon ionization amplitudes. The interference term can be given by [57–59]

$$\mathcal{A}^{(1,2)}(t) = 2\mathcal{W}^{(1)}(t)\mathcal{W}^{(2)}(t)\cos(\eta), \tag{5}$$

where $\mathcal{W}^{(1)}$ and $\mathcal{W}^{(2)}$ are respectively the transition matrix elements for the two ω ($\omega+\omega$) and one 2ω photoionization processes, which are determined by the driving laser pulses, and η is the phase of the coherent electron wave packets. The corresponding laser-induced electron angular current $j_\theta(\mathbf{r},t)$ is expressed as [34,35]

$$\frac{d}{dt}\mathcal{A}^{(1,2)}(t) + \frac{\partial}{\partial\theta} j_\theta(t) = 0. \tag{6}$$

In Eq. (6), the angular electron current $j_\theta(t)$ is shown to be dependent on the transition interference term $\mathcal{A}^{(1,2)}$. As shown in Eq. (4), the generated magnetic field arises from the electron current, $B(t) \sim j_\theta(t)$. Therefore during the photoexcitation and ionization processes, the induced magnetic field $B_z(\mathbf{r}=0,t)$ is modulated by the interference effects in Eq. (5), as illustrated in Fig. 4. However, for the case at $\lambda = 70$ nm, the contribution of generated magnetic fields from the interference term $\mathcal{A}^{(1,2)}$ is negligible since the strong $1s\sigma_g$–$2p\pi_u$ resonant excitation dominates, thus leading to similar time-dependent magnetic fields in Fig. 3. The dependence of the generated magnetic field $B_z(\mathbf{r}=0,t)$ on the pulse frequency combination illustrates the difference of the coherent excitation-ionization processes. As illustrated in Fig. 1, the excited-state orbitals (m) are different for different excitation processes. Therefore, varying the molecular alignments and the pulse frequency and helicity combinations gives rise to a strong modulation of the spatial distributions of the generated magnetic field, as discussed next.

B. Spatially resolved attosecond magnetic field distributions

We next present the spatial evolution of the generated attosecond magnetic fields. Figures 5 and 6 display the density distributions of the generated magnetic field $B_z(\mathbf{r},t)$ in the two planes, $(x, y, z=0)$ and $(x, y=0, z)$, by bichromatic counterrotating $(\omega, 2\omega)$ circularly polarized laser pulses at different moments (from left to right panels) $t = 2.0$ oc, 2.25 oc, 2.5 oc, and 2.75 oc with a time interval of 0.25 oc. We plot the distributions for the two cases, in Fig. 5 the molecular alignments along the x axis, and the z axis in Fig. 6, i.e., the molecular axis is parallel [in plane, Fig. 1(a)] and perpendicular [around axis, Fig. 1(b)] to the laser (x, y) polarization plane. The bichromatic $(\omega, 2\omega)$ counterrotating circularly polarized pulse wavelengths are (a) 70 nm and 35 nm, and (b) 100 nm and 50 nm, with respectively π_u and σ_u resonant excitation. It is found that the generated field $B(\mathbf{r},t)$ evolves periodically with time, following the driving electric field. The evolution of the generated magnetic fields with time is in good agreement with the results in Figs. 3 and 4.

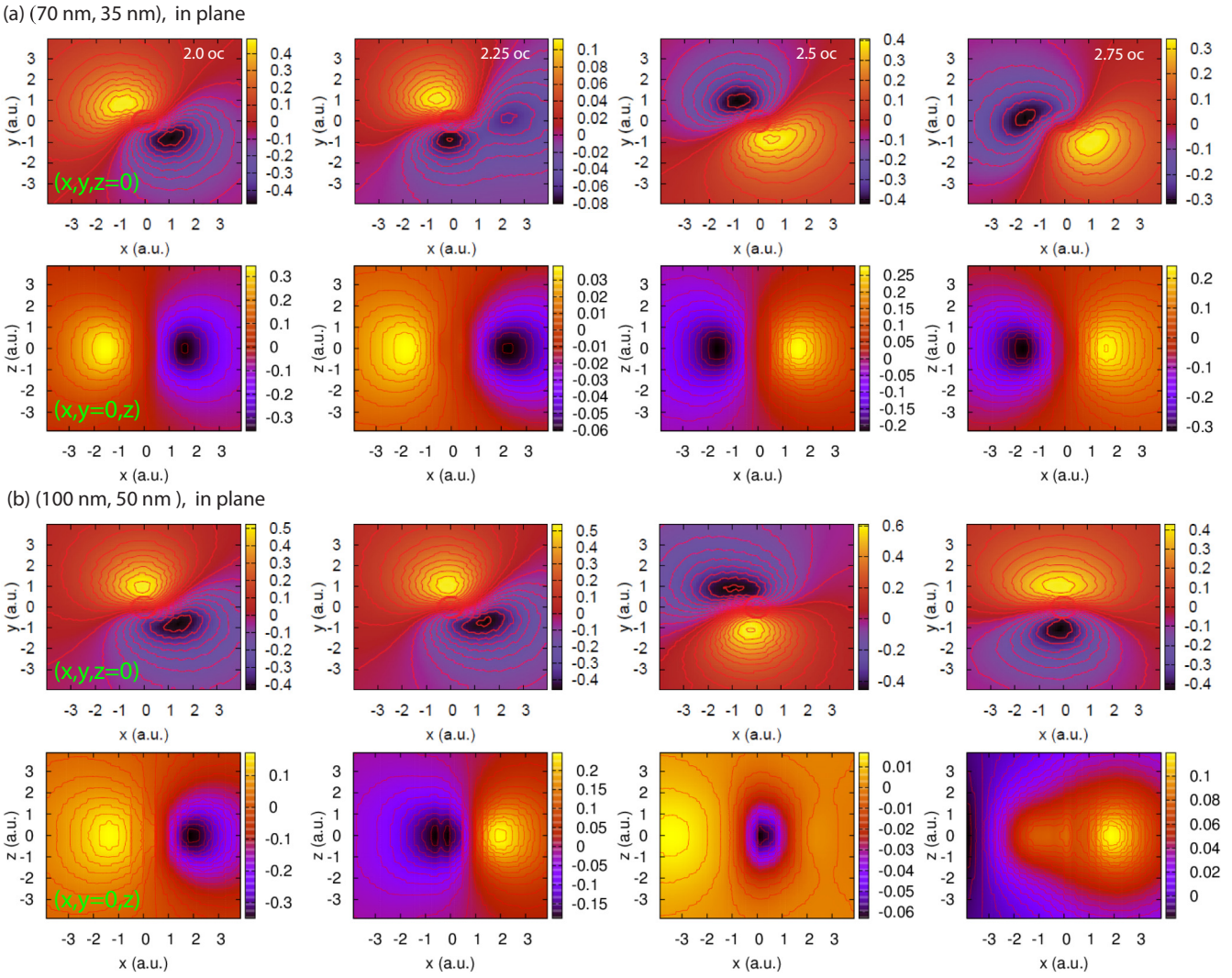

FIG. 5. Density plots of spatiotemporal magnetic fields $B_z(\mathbf{r}, t)$ in the $(x, y, z = 0)$ and $(x, y = 0, z)$ planes at different moments (from left to right) $t = 2.0$ oc, 2.25 oc, 2.5 oc, and 2.75 oc, where 1 optical cycle (oc) $= 2\pi/\omega$. Two cases of the bichromatic $(\omega, 2\omega)$ counterrotating circularly polarized laser pulses with their field vectors in the molecular (x, y) plane [in plane, Fig. 1(a)] are presented. The pulse wavelengths are, respectively, (a) (70 nm, 35 nm) and (b) (100 nm, 50 nm); cf. Figs. 3(a) and 4(a).

The spatial distributions of the generated magnetic field in the $(x, y, z = 0)$ plane reflect the symmetry of the molecular orbitals of the excited states. For the process by the bicircular 70 nm and 35 nm pulse, the $1s\sigma_g$–$2p\pi_u$ resonant excitation dominates with π_u symmetry. For the in-plane case with $R \parallel x$, the excited electronic states are degenerate with $m = \pm 1$. The perpendicular excitation therefore leads to an oscillation of the generated magnetic field $B_z(x, y)$ in the up $(y > 0)$ and down $(y < 0)$ half planes, perpendicular to the molecular R/x axis, in Fig. 5(a). For the around-axis case, the excited-state orbital is given in the cylindrical coordinates, Fig. 1, $\psi_{\pi_u} = \psi_x + i\psi_y = \psi(x, y)e^{im\theta}$, $m = 1$. The electronic density distributions are localized around the molecular axis. As a result, the time-dependent magnetic field $B_z(\mathbf{r}, t)$ shows a rotation around the molecular R axis in Fig. 6(a). For the bichromatic 100 nm and 50 nm pulse, the different molecular alignments give rise to various excitation processes. Such few cycle pulses with broad spectral widths produce dense excited Rydberg states below the molecular ionization potential since $2\omega < I_p$, where I_p is the molecular ionization potential. In the case of the molecule aligned along the z axis, i.e., the around-axis case in Fig. 1(b), the excited states have respective π_u symmetry with $m = 1$ and δ_g symmetry with $m = 2$ after one 2ω and two ω, $(\omega + \omega)$, photon absorptions. Since the excited electronic state wave functions are a function of the azimuthal angle $e^{im\theta}$, the magnetic fields also evolve around the molecular R axis, in Fig. 6(b), similar to those in Fig. 6(a). For the process of the molecule aligned along the x axis, i.e., the in-plane case in Fig. 1(a), the σ_g-σ_u parallel resonant excitation occurs for the 100 nm pulse. In the bichromatic circularly polarized pulse with wavelengths 100 nm and 50 nm, this process is composed of two-pathway excitation processes, a single 2ω photon process and a ladder excitation $\pi_g \leftarrow \sigma_u \leftarrow \sigma_g$. The two-pathway processes can be regarded as two single photon perpendicular excitation processes from, respectively, the $1s\sigma_g$ and the $2p\sigma_u$ electronic states. The excited electronic states are degenerate with $m = \pm 1$. Consequently, one obtains that the magnetic field oscillates in the up-down plane,

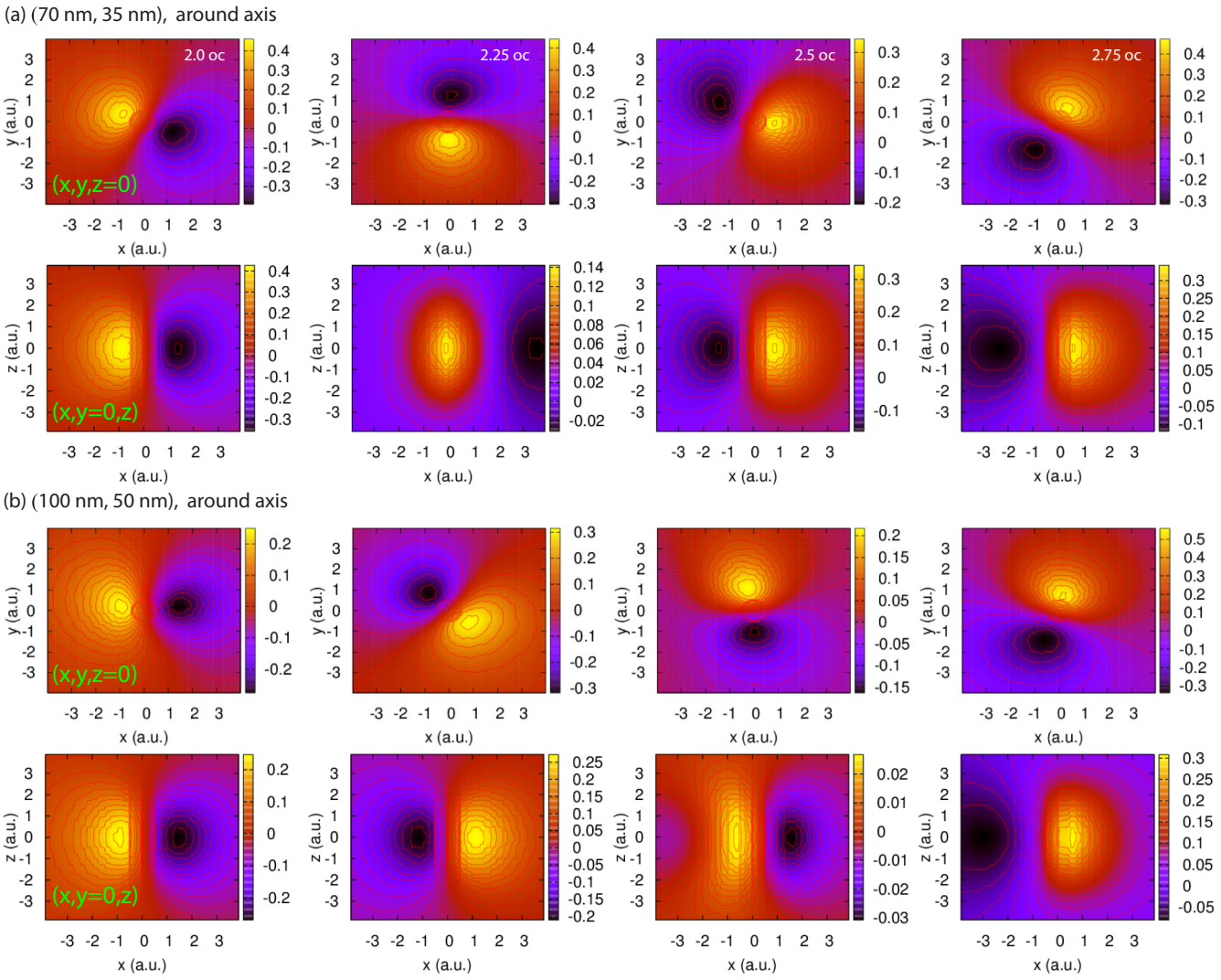

FIG. 6. Density plots of spatiotemporal magnetic fields $B_z(\mathbf{r}, t)$ in the $(x, y, z = 0)$ and $(x, y = 0, z)$ planes at different moments (from left to right) $t = 2.0$ oc, 2.25 oc, 2.5 oc, and 2.75 oc, where 1 optical cycle (oc) $= 2\pi/\omega$. Two cases of the bichromatic $(\omega, 2\omega)$ counterrotating circularly polarized laser pulses with their field vectors perpendicular to the molecular R/z axis [around axis, Fig. 1(b)] are presented. The pulse wavelengths are, respectively, (a) (70 nm, 35 nm) and (b) (100 nm, 50 nm); cf. Figs. 3(b) and 4(b).

in Fig. 5(b). The evolution of the time-dependent magnetic field $B_z(x, y, z = 0, t)$ reflects the degeneracy of the excited electronic states.

The generated magnetic fields are mainly localized along the z axis, perpendicular to the (x, y) currents, as predicted by classical physics [60]. In the present molecular case, the evolution of the generated magnetic field with time results from the corresponding time-dependent induced electron currents, i.e., coherent electron wave packets, for which a semiclassical model provides estimates of the radii of the circular electron currents at single frequencies ω and field amplitudes E_0 [61]. Assuming zero initial electron velocities, maximum induced electron velocities $v = 2E_0/\omega$ give circular radii

$$r_n = \frac{2E_0}{\omega^2}\sqrt{1 + \left(n + \frac{1}{2}\right)^2 \pi^2}, \quad n = 0, 1, 2, \ldots, \tag{7}$$

at times $t = (2n + 1)\pi/\omega$. Thus at $I_x = I_y = 3.5 \times 10^{14}$ W/cm^2 ($E_0 = 0.1$ a.u.), one obtains at $\lambda = 70$ nm, $r_0 = 0.87$ a.u. and $r_1 = 2.27$ a.u., and at $\lambda = 100$ nm, $r_0 = 1.8$ a.u. and $r_1 = 4.6$ a.u. Short cycles $n = 0$ give the largest magnetic fields due to small radii at shorter time t_n.

For the in-plane case, Fig. 5, the protons are situated at $x = \pm R/2 = \pm 1$ a.u. The magnetic fields B_z are maximum at $z = 0$, i.e., along the x-aligned R nuclear axis, but appear generally at each proton, with different phases. Similarly around the z axis, parallel to R, the protons are situated at $z = \pm R/2 = \pm 1$ a.u. As shown in Fig. 6, the magnetic field lies at positions with maximum values of $x = 0.9$ a.u. for the (70 nm, 35 nm) process and $x = 1.6$ a.u. for the (100 nm, 50 nm) process. For example, at time 2.75 oc, one finds that the maximum magnetic field B_z appears at position (0,0.9,0) a.u. in Fig. 6(a) and at $(-1.6, 0, 0)$ a.u. in Fig. 6(b). The maximum displacements of the magnetic fields depend on the pulse wavelengths, reflecting the dimensions of the laser-induced electron currents, predicted from Eq. (7). In the circular laser field at frequency ω and field strength E_0, the first maximum laser-induced electron radius is given by the semiclassical

ionization model. At $\lambda = 70$ nm, the corresponding radius is $r_0 = 0.87$ a.u., and at $\lambda = 100$ nm, $r_0 = 1.8$ a.u., in agreement with the numerical simulations, where the electron rotates around the molecular R axis with radius r_0 in the $(x, y, z = 0)$ plane, in Fig. 6.

However, for the in-plane case in Fig. 5, the displacements of the generated magnetic field are slightly larger than those in Fig. 6. The difference results from Coulomb effects from the two nuclei. Figure 5 shows that the magnetic-field distributions mainly lie around the two molecular proton centers; i.e., the maxima $B_z(x, y = 0, z)$ occur around $x = \pm R/2 = \pm 1$, as illustrated in the $(x, y = 0, z)$ plane. According to molecular orbital theory, the molecular wave function is a linear combination of the atomic configurations, i.e., $\psi(\mathbf{r}) = [\psi_R(\mathbf{r} = \mathbf{R}/2) + \psi_L(\mathbf{r} = -\mathbf{R}/2)]/\sqrt{2}$, where $\psi_R(\mathbf{r} = \mathbf{R}/2)$ and $\psi_L(\mathbf{r} = -\mathbf{R}/2)$ denote the wave functions of the atomic orbital on the left $\mathbf{r} = -\mathbf{R}/2$ and right $\mathbf{r} = \mathbf{R}/2$ protons. From Eqs. (3) and (4) one sees that the generated magnetic field depends on the electron wave function, i.e., $B \sim \psi \nabla \psi$, giving rise to the maxima of $B_z(-R/2, y, z)$ and $B_z(+R/2, y, z)$ with opposite phases [33]. At the molecular center, the magnetic field is a simple sum of the two parts on the two protons with opposite phase, i.e., $B_z(\mathbf{r} = 0, t) = B_z(\mathbf{r} = \mathbf{R}/2, t) + B_z(\mathbf{r} = -\mathbf{R}/2, t)$. Due to the helicity effects of the circular polarization field, the generated magnetic fields on the two proton are not equivalent, $B_z(\mathbf{r} = \mathbf{R}/2, t) \neq B_z(\mathbf{r} = -\mathbf{R}/2, t)$. Magnetic fields are generated at the molecular center at $\mathbf{r} = 0$, as shown in Figs. 3 and 4. As a consequence of the induced electron currents, the generated magnetic fields evolve around the molecule with radii $r_0' = R/2 + r_0 = 2.0$ a.u. at $\lambda = 70$ nm and 35 nm and $r_0' = 3$ a.u. at $\lambda = 100$ nm and 50 nm, as illustrated in Figs. 5(a) and 5(b). Of note is that, in these cases, the molecular axis is perpendicular to the $(x = 0, y, z)$ plane. The two center effects do not influence the spatial $(x = 0, y, z)$ distributions of the generated magnetic field. As a result, the evolution of $B(x = 0, y, z, t)$ is similar to those around the axis.

The spatiotemporal evolution of the induced magnetic field illustrated in Figs. 5 and 6 reflects electron coherence. As mentioned above, the resonant excitation between the ground $1s\sigma_g$ electronic state and the excitation electronic state with different orbital momentum m induces coherent angular electron current, j_θ, therefore leading to ultrafast magnetic-field generation in Figs. 3–6. The dependence of the generated magnetic field on the pulse frequency and helicity and the molecular alignment indicates the property of the coherent resonant excitation induced by the bichromatic circularly polarized pulses. The observed magnetic-field distributions are mapped from the induced electron currents. Therefore, the coherent excitation encoded in the electron currents can be reconstructed with spatial and temporal resolutions by the generated magnetic field.

IV. SUMMARY

We present spatial and temporal evolution of the magnetic-field-pulse generation in molecules by intense bichromatic circularly polarized UV laser pulses. The single-electron diatomic H_2^+ is used as a benchmark model system since it can be fully and accurately investigated in both theory and experiment [42]. Results from numerical solutions of the molecular TDSE show that generated magnetic field pulses are dependent on the molecular alignments and pulse frequency and helicity combinations. We simulate the magnetic field in two cases of molecular alignments, parallel and perpendicular to the laser polarization plane (Fig. 1), at different pulse frequency $\lambda = 70$ nm resonant with π_u orbitals and 100 nm resonant with σ_u orbitals and helicity (corotating and counterrotating) combinations.

The results show that the time-dependent generated magnetic fields are modulated in bichromatic circularly polarized pulses due to interference effects of coherent circular electron wave packets. The modulation of the generated magnetic field is also sensitive to the molecular alignment and the pulse frequency and helicity combinations. At different pulse frequency combinations, different resonant excitation processes give rise to various electron currents and magnetic fields. In the 100 nm cases, the electron currents arising from the double resonant excitations by two ω and one 2ω with different rotating components interfere with each other. Moreover, the excited-state orbitals and corresponding coherent electron currents depend on the pulse helicity, as illustrated in Fig. 1. Consequently, the magnetic field oscillates strongly with time, which is a function of the pulse frequency and helicity combination, in Fig. 4. The magnetic fields for the corotating and counterrotating components evolve generally with opposite phases. However, in the 70 nm cases, the $1s\sigma_g$–$2p\pi_u$ resonant excitation dominates and the interference effects between multiphoton excitation processes are negligible. As a consequence of dominant single ω resonant excitations, the coherent interference effects are absent and the magnetic field exhibits similar evolution processes at different pulse frequency combinations, as shown in Fig. 3.

Generation of ultrafast magnetic field pulses by single-frequency few-cycle circularly polarized pulses has been shown to be stable with respect to bichromatic excitation schemes at frequencies resonant with π orbitals ($\Delta m = \pm 1$ transition) in molecules. Excitations of electron currents with definite angular momentum both around the molecular internuclear axis or in plane thus generate magnetic fields that remain invariant to multiple-frequency excitations. Nevertheless, the in-plane currents generate magnetic fields that change phases in the middle of the duration of all pulses, single and corotating/counterrotating bichromatic circularly polarized pulses. Excitations of σ orbitals ($\Delta m = 0$ transition) occur with intense resonant circular polarized pulses preferentially in molecule-laser polarization parallel alignments, due to strong charge resonance electronic transitions parallel to the internuclear axis. The in-plane currents for the latter parallel alignments undergo strong Coulomb interactions with nuclei, producing stronger corotating and counterrotating laser-induced magnetic fields than single-frequency excitations, but with phases oscillating at twice the lower laser frequency. Of note is that in this in-plane parallel laser-molecule alignment, corotating bichromatic pulses lead to magnetic fields out of phase with counterrotating combinations at magnetic-field maxima-minima (n oc), whereas corotating $(\omega, 3\omega)$ and counterrotating $(\omega, 2\omega)$ maxima-minima are in phase at half cycles, i.e., $(2n + 1)/2$ oc. These results, resonant π vs σ orbital in-plane excitation with single vs bichromatic

circularly polarized pulse, emphasize the importance of electron current–nuclear interactions. In such molecule-laser polarization parallel alignments, i.e., in plane, bichromatic circularly polarized pulses generate generally more intense ultrafast magnetic fields than by single-frequency pulses, but with phases that vary at single (ω) and twice single (2ω) laser frequencies. The present results in principle pave a way to generate and control ultrafast magnetic fields by bichromatic circularly polarized laser pulses, which can be extended to other complex molecular systems for studying electron dynamics in ultrafast magneto-optics [62] and molecular chiral properties [63].

ACKNOWLEDGMENTS

J.G. acknowledges support from National Natural Science Foundation of China under Grant No. 11574117. We also thank Compute Canada for access to massively parallel computer clusters, and NSERC and FQRNT for support of this research.

[1] F. Krausz and M. Ivanov, Attosecond physics, Rev. Mod. Phys. **81**, 163 (2009).
[2] Z. Chang, P. B. Corkum, and S. R. Leone, Attosecond optics and technology: Progress to date and future prospects, J. Opt. Soc. Am. B **33**, 1081 (2016).
[3] T. Gaumnitz, A. Jain, Y. Pertot, M. Huppert, I. Jordan, F. Ardana-Lamas, and H. J. Wörner, Streaking of 43-attosecond soft-x-ray pulses generated by a passively CEP-stable mid-infrared driver, Opt. Express **25**, 27506 (2017).
[4] T. Popmintchev *et al.*, Bright coherent ultrahigh harmonics in the keV x-ray regime from mid-infrared femtosecond lasers, Science **336**, 1287 (2012).
[5] S. Chelkowski, G. L. Yudin, and A. D. Bandrauk, Observing electron motion in molecules, J. Phys. B **39**, S409 (2006).
[6] H. Niikura, D. M. Villeneuve, and P. B. Corkum, Mapping Attosecond Electron Wave Packet Motion, Phys. Rev. Lett. **94**, 083003 (2005).
[7] H. C. Shao and A. F. Starace, Detecting Electron Motion in Atoms and Molecules, Phys. Rev. Lett. **105**, 263201 (2010).
[8] M. J. J. Vrakking and T. E. Elsasser, X-ray photonics: X-rays inspire electron movies, Nat. Photonics **6**, 645 (2012).
[9] P. M. Kraus *et al.*, Measurement and laser control of attosecond charge migration in ionized iodoacetylene, Science **350**, 790 (2015).
[10] P. Lan, M. Ruhmann, L. He, C. Zhai, F. Wang, X. Zhu, Q. Zhang, Y. Zhou, M. Li, M. Lein, and P. Lu, Attosecond Probing of Nuclear Dynamics with Trajectory-Resolved High-Harmonic Spectroscopy, Phys. Rev. Lett. **119**, 033201 (2017).
[11] X. Wang and J. H. Eberly, Effects of Elliptical Polarization on Strong-Field Short-Pulse Double Ionization, Phys. Rev. Lett. **103**, 103007 (2009).
[12] X. Wang and J. H. Eberly, Elliptical Polarization and Probability of Double Ionization, Phys. Rev. Lett. **105**, 083001 (2010).
[13] F. Mauger, C. Chandre, and T. Uzer, From Recollisions to the Knee: A Road Map for Double Ionization in Intense Laser Fields, Phys. Rev. Lett. **104**, 043005 (2010).
[14] F. Mauger, C. Chandre, and T. Uzer, Recollisions and Correlated Double Ionization with Circularly Polarized Light, Phys. Rev. Lett. **105**, 083002 (2010).
[15] K. J. Yuan, C. C. Shu, D. Dong, and A. D. Bandrauk, Attosecond dynamics of molecular electronic ring currents, J. Phys. Chem. Lett. **8**, 2229 (2017).
[16] K. J. Yuan and A. D. Bandrauk, Exploring coherent electron excitation and migration dynamics by electron diffraction with ultrashort x-ray pulses, Phys. Chem. Chem. Phys. **19**, 25846 (2017).
[17] A. D. Bandrauk, J. Guo, and K. J. Yuan, Circularly polarized attosecond pulse generation and applications to ultrafast magnetism, J. Opt. **19**, 124016 (2017).
[18] P. B. Corkum, Plasma Perspective on Strong Field Multiphoton Ionization, Phys. Rev. Lett. **71**, 1994 (1993).
[19] T. Zuo and A. D. Bandrauk, High-order harmonic generation in intense laser and magnetic fields, J. Nonlinear Opt. Phys. Mater. **04**, 533 (1995).
[20] S. Long, W. Becker, and J. K. McIver, Model calculations of polarization-dependent two-color high-harmonic generation, Phys. Rev. A **52**, 2262 (1995).
[21] X.-M. Tong and S.-I. Chu, Generation of circularly polarized multiple high-order harmonic emission from two-color crossed laser beams, Phys. Rev. A **58**, R2656(R) (1998).
[22] D. B. Milošević, W. Becker, and R. Kopold, Generation of circularly polarized high-order harmonics by two-color coplanar field mixing, Phys. Rev. A **61**, 063403 (2000).
[23] T. Fan *et al.*, Bright circularly polarized soft x-ray high harmonics for x-ray magnetic circular dichroism, Proc. Natl. Acad. Sci. USA **112**, 14206 (2015).
[24] A. D. Bandrauk, F. Mauger, and K. J. Yuan, Circularly polarized harmonic generation by intense bicircular laser pulses: Electron recollision dynamics and frequency-dependent helicity, J. Phys. B **49**, 23LT01 (2016).
[25] K. J. Yuan and A. D. Bandrauk, Single Circularly Polarized Attosecond Pulse Generation by Intense Few Cycle Elliptically Polarized Laser Pulses and Terahertz Fields from Molecular Media, Phys. Rev. Lett. **110**, 023003 (2013).
[26] A. Tsiatmas, E. Atmatzakis, N. Papasimakis, V. Fedotov, B. Lukyanchuk, N. I. Zheludev, and F. J. García de Abajo, Optical generation of intense ultrashort magnetic pulses at the nanoscale, New J. Phys. **15**, 113035 (2013).
[27] J.-Y. Bigot, M. Vomir, and E. Beaurepaire, Coherent ultrafast magnetism induced by femtosecond laser pulses, Nat. Phys. **5**, 515 (2009).
[28] G. P. Zhang, W. Hübner, G. Lefkidis, Y. Bai, and T. F. George, Paradigm of the time-resolved magneto-optical Kerr effect for femtosecond magnetism, Nat. Phys. **5**, 499 (2009).
[29] K. Nobusada and K. Yabana, Photoinduced electric currents in ring-shaped molecules by circularly polarized laser pulses, Phys. Rev. A **75**, 032518 (2007).
[30] M. Kanno, H. Kono, Y. Fujimura, and S. H. Lin, Nonadiabatic Response Model of Laser-Induced Ultrafast π-Electron Rotations in Chiral Aromatic Molecules, Phys. Rev. Lett. **104**, 108302 (2010).

[31] I. Barth, J. Manz, Y. Shigeta, and K. Yagi, Unidirectional electronic ring current driven by a few cycle circularly polarized laser pulse: Quantum model simulations for Mg-porphyrin, J. Am. Chem. Soc. **128**, 7043 (2006).

[32] I. Barth and J. Manz, Electric ring currents in atomic orbitals and magnetic fields induced by short intense circularly polarized π laser pulses, Phys. Rev. A **75**, 012510 (2007).

[33] K. J. Yuan, J. Guo, and A. D. Bandrauk, Generation of ultrafast magnetic fields from molecular coherent electron currents, Phys. Rev. A **98**, 043410 (2018).

[34] G. Hermann, C. Liu, J. Manz, B. Paulus, J. F. Perez- Torres, V. Pohl, and J. C. Tremblay, Multidirectional angular electronic flux during adiabatic attosecond charge migration in excited benzene, J. Phys. Chem. A **120**, 5360 (2016).

[35] D. Jia, J. Manz, B. Paulus, V. Pohl, J. C. Tremblay, and Y. Yang, Quantum control of electronic fluxes during adiabatic attosecond charge migration in degenerate superposition states of benzene, Chem. Phys. **482**, 146 (2017).

[36] C. Liu, J. Manz, K. Ohmori, C. Sommer, N. Takei, J. C. Tremblay, and Y. Zhang, Attosecond Control of Restoration of Electronic Structure Symmetry, Phys. Rev. Lett. **121**, 173201 (2018).

[37] C. Liu, J. Manz, and J. C. Tremblay, From symmetry breaking via charge migration to symmetry restoration in electronic ground and excited states: Quantum control on the attosecond time scale, Appl. Sci. **9**, 953 (2019).

[38] K. J. Yuan and A. D. Bandrauk, Attosecond-magnetic-field-pulse generation by intense few-cycle circularly polarized UV laser pulses, Phys. Rev. A **88**, 013417 (2013).

[39] K. J. Yuan and A. D. Bandrauk, Attosecond-magnetic-field-pulse generation by coherent circular molecular electron wave packets, Phys. Rev. A **91**, 042509 (2015).

[40] K. J. Yuan and A. D. Bandrauk, Attosecond-magnetic-field-pulse generation by electronic currents in bichromatic circularly polarized UV laser fields, Phys. Rev. A **92**, 063401 (2015).

[41] X. Zhang, X. Zhu, D. Wang, L. Li, X. Liu, Q. Liao, P. Lan, and P. Lu, Ultrafast oscillating-magnetic-field generation based on electronic-current dynamics, Phys. Rev. A **99**, 013414 (2019).

[42] H. Ibrahim, C. Lefebvre, A. D. Bandrauk, A. Staudte, and F. Légaré, H_2: The benchmark molecule for ultrafast science and technologies, J. Phys. B **51**, 042002 (2018).

[43] K.-J. Yuan and A. D. Bandrauk, Symmetry in circularly polarized molecular high-order harmonic generation with intense bicircular laser pulses, Phys. Rev. A **97**, 023408 (2018).

[44] A. D. Bandrauk and K. J. Yuan, Molecular electron recollision dynamics in intense circularly polarized laser pulses, J. Phys. B **51**, 074001 (2018).

[45] D. Baykusheva, M. S. Ahsan, N. Lin, and H. J. Wörner, Bicircular High-Harmonic Spectroscopy Reveals Dynamical Symmetries of Atoms and Molecules, Phys. Rev. Lett. **116**, 123001 (2016).

[46] D. M. Reich and L. B. Madsen, Illuminating Molecular Symmetries with Bicircular High-Order-Harmonic Generation, Phys. Rev. Lett. **117**, 133902 (2016).

[47] J. M. Ngoko Djiokap, S. X. Hu, L. B. Madsen, N. L. Manakov, A. V. Meremianin, and A. F. Starace, Electron Vortices in Photoionization by Circularly Polarized Attosecond Pulses, Phys. Rev. Lett. **115**, 113004 (2015).

[48] D. Pengel, S. Kerbstadt, D. Johannmeyer, L. Englert, T. Bayer, and M. Wollenhaupt, Electron Vortices in Femtosecond Multiphoton Ionization, Phys. Rev. Lett. **118**, 053003 (2017).

[49] K. J. Yuan, S. Chelkowski, and A. D. Bandrauk, Photoelectron momentum distributions of molecules in bichromatic circularly polarized attosecond UV laser fields, Phys. Rev. A **93**, 053425 (2016).

[50] A. D. Bandrauk, F. Fillion-Gourdeau, and E. Lorin, Atoms and molecules in intense laser fields: Gauge invariance of theory and models, J. Phys. B **46**, 153001 (2013).

[51] A. D. Bandrauk and H. Shen, Exponential split operator methods for solving coupled time–dependent Schrödinger equations, J. Chem. Phys. **99**, 1185 (1993).

[52] K. J. Yuan, H. Z. Lu, and A. D. Bandrauk, Circular-polarization photoionization angular distributions in H_2 and H_2^+ by attosecond xuv laser pulses, Phys. Rev. A **83**, 043418 (2011).

[53] O. D. Jefimenko, *Electricity and Magnetism: An Introduction to the Theory of Electric and Magnetic Fields* (Electret Scientific Co., Star City, 1989).

[54] R. S. Mulliken, Low electronic states of simple heteropolar diatomic molecules: III. Hydrogen and univalent metal halides, Phys. Rev. **51**, 310 (1937).

[55] T. Zuo and A. D. Bandrauk, Charge-resonance-enhanced ionization of diatomic molecular ions by intense lasers, Phys. Rev. A **52**, R2511 (1995).

[56] W. Lai and C. Guo, Polarization and molecular-orbital dependence of strong-field enhanced ionization, Phys. Rev. A **93**, 043401 (2016).

[57] E. A. Pronin, A. F. Starace, M. V. Frolov, and N. L. Manakov, Perturbation theory analysis of attosecond photoionization, Phys. Rev. A **80**, 063403 (2009).

[58] E. A. Pronin, A. F. Starace, and L. Y. Peng, Perturbation-theory analysis of ionization by a chirped few-cycle attosecond pulse, Phys. Rev. A **84**, 013417 (2011).

[59] K.-J. Yuan and A. D. Bandrauk, Molecular above-threshold-ionization angular distributions with attosecond bichromatic intense XUV laser pulses, Phys. Rev. A **85**, 013413 (2012).

[60] D. Halliday, R. Resnick, and J. Walker, *Fundamentals of Physics* (Wiley, New York, 1961), Chap. 37.

[61] K. J. Yuan and A. D. Bandrauk, Circularly polarized attosecond pulses from molecular high-order harmonic generation by ultrashort intense bichromatic circularly and linearly polarized laser pulses, J. Phys. B **45**, 074001 (2012).

[62] G. P. Zhang and T. F. George, Total angular momentum conservation in laser-induced femtosecond magnetism, Phys. Rev. B **78**, 052407 (2008).

[63] O. Neufeld and O. Cohen, Optical Chirality in Nonlinear Optics: Application to High Harmonic Generation, Phys. Rev. Lett. **120**, 133206 (2018).